Modeling dynamics of AIR-1, ECT-2, and myosin in polarity establishment and cytokinesis

Ondrej Maxian

March 11, 2024

1 The centrosome cue

The contractility circuit is forced by a cue from the centrosomes which contain Aurora A (AIR-1), an inhibitor of ECT-2. We assume that the AIR-1 signal gets to the membrane by diffusion. Letting $a(\boldsymbol{x})$ be the concentration of AIR-1 in the embryo, we have the equation

$$\Delta a = -f \qquad \boldsymbol{x} \in \Omega \tag{1a}$$

$$\nabla a \cdot \boldsymbol{n} = 0 \quad \boldsymbol{x} \in \partial\Omega, \tag{1b}$$

where (1a) is the diffusion equation for the concentration and (1b) is a no-flux boundary condition through the boundary (here Ω represents the embryo area and $\partial\Omega$ represents the boundary). The signal $f(\boldsymbol{x})$ comes from the two centrosomes, which we model by Gaussian densities

$$f(\boldsymbol{x}) = \frac{C_0/D}{2\pi\sigma_c^2} \sum_{i=1}^{2} \exp\left(\frac{-\|\boldsymbol{x}-\boldsymbol{x}_i\|^2}{2\sigma_c^2}\right). \tag{1c}$$

Here $\boldsymbol{x}_i$ is the location of the ith centrosome (typically at some location $(x_i, 0)$), which changes depending on the embryo conditions. In addition to the centrosome location, the signal has two other parameters: C_0/D is the strength of the cue (the integral of $f(\boldsymbol{x})$ over the entire embryo cross-section, normalized by the cytoplasmic diffusion coefficient D), and σ_c is the centrosome "size" (the standard deviation of the Gaussian, which is roughly half the size of the centrosome). For cytokinesis, the centrosomes have size about 2 μm, so we set $\sigma_c = 1$ μm. The solution of (1a) is unique up to a constant; thus, when we compare profiles to each other we can only speak of concentration *differences* rather than absolute concentration.

We use a standard first-order finite element method to solve (1a). In brief, the elliptical domain of the embryo is meshed into nodes and triangles, which define a set of linear Lagrangian basis

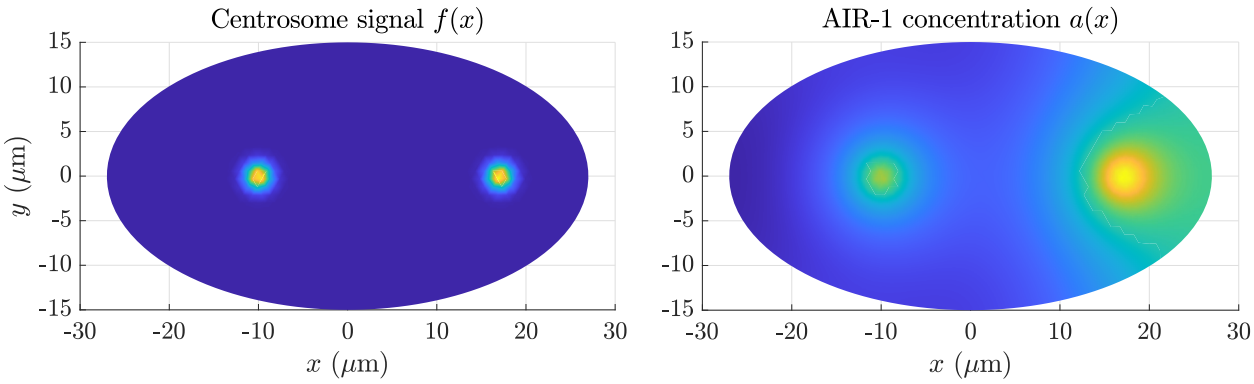

Figure 1: Solution for the diffusion equation (1) for wild-type embryos. The left panel shows the centrosome signal $f(\boldsymbol{x})$, with the anterior centrosome 17 μm away from the anterior cortex and the posterior centrosome 10 μm away from the posterior cortex. The Gaussian width $\sigma_c = 1$ (so that the centrosome diameter is roughly 2 μm). The right panel shows the solution for the concentration profile $a(\boldsymbol{x})$.

functions ψ_k that are 1 at node $\boldsymbol{x}_k$ and 0 everywhere else. Multiplying (1a) by a basis function ψ_k, then integrating by parts using the boundary condition (1b) gives

$$\sum_j \int_\Omega (\nabla \psi_k \cdot \nabla \psi_j)\, a_j \, d\boldsymbol{x} = \sum_j \int_\Omega \psi_k \psi_j f_j \, d\boldsymbol{x}, \tag{2}$$

which can be written as the matrix equation $\boldsymbol{K}\boldsymbol{a} = \boldsymbol{M}\boldsymbol{f}$, where $\boldsymbol{M}$ is the so-called mass matrix and $\boldsymbol{K}$ the stiffness matrix for finite elements. Solving $\boldsymbol{a} = \boldsymbol{K}^\dagger \boldsymbol{M}\boldsymbol{f}$ gives the solution for the concentration.

Figure 1 shows the solution of the diffusion equation over the embryo cross-section in wild-type embryos. In this case, the anterior centrosome sits 17 μm from the anterior pole, while the posterior centrosome sits 10 μm from the posterior pole. The left panel shows the AIR-1 signal, which essentially shows the location of the two centrosomes. The right panel then shows the solution to the diffusion equation (1) in this case. As might be expected, there is substantially more AIR-1 on the anterior cortex, since the centrosome sits closer to the boundary there.

We now consider how moving the centrosomes changes the profile of AIR-1 on the boundary. We use six representative treatments from [5], which modify the positions of the centrosomes, and plot the results in Fig. 2. As an example, in dhc-1 (RNAi) embryos, the posterior centrosome sits 3 μm from the posterior pole, while the anterior centrosome sits 45 μm from the anterior pole (9 μm from the posterior pole). As a result, the AIR-1 profile is strongly peaked at the posterior, with an AIR-1 gradient about 6 times larger than the wild-type. The treatments we consider

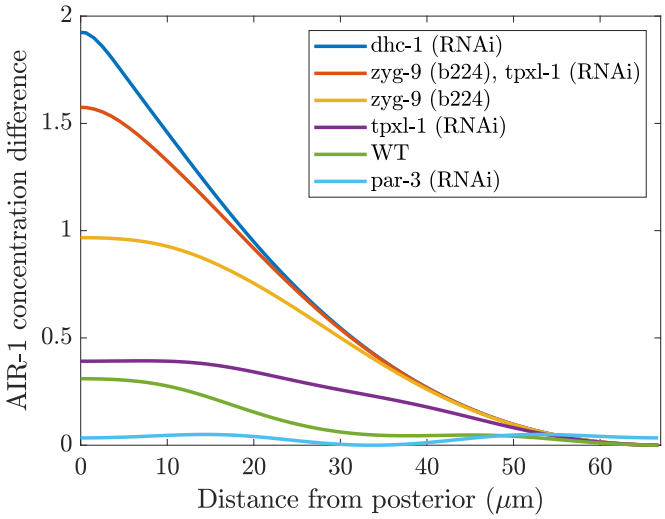

Figure 2: AIR-1 accumulation on the embryo perimeter (cortex) as predicted by the diffusion model (1). We show the AIR-1 profile as a function of distance from the posterior pole (0 is the posterior pole, 67 is the anterior pole), for embryos with six different treatments. The treatment sets the location of the centrosomes (see Fig. 5).

can also flatten the AIR-1 profile relative to wild-type, as in PAR-3 (RNAi) embryos, which have centrosomes sitting roughly at 15 μm from each pole. The profile of AIR-1 there is consequently roughly constant.

1.1 Adding AIR-1 inactivation

We also consider the case when there is a basal level of inactivation of AIR-1 in the cytoplasm. To model this, we modify (1a) to add an additional inactivation term

$$\Delta a - \bar{k}^{\text{off}} a = -f \qquad \boldsymbol{x} \in \Omega. \tag{3}$$

This introduces another parameter which is the inactivation rate relative to the diffusion coefficient in the cytoplasm (units μm^{-2}). Solving (3) with the finite element is very simple: the matrix equation becomes $\left(\boldsymbol{K} + \bar{k}^{\text{off}}\boldsymbol{M}\right)\boldsymbol{a} = \boldsymbol{M}\boldsymbol{f}$. An advantage of this approach is that the solution for concentration is unique (no longer an unknown constant).

Figure 3 shows the effect of the new inactivation term in the model, both in the cross-sectional profile of AIR-1, and also along the embryo perimeter from posterior to anterior. We find that $\bar{k}^{\text{off}} \leq 10^{-3}$ μm^{-2} preserves the general trend we observed previously in wild-type embryos, where the concentration is about 0.3 units higher at the posterior than the anterior. Increasing the

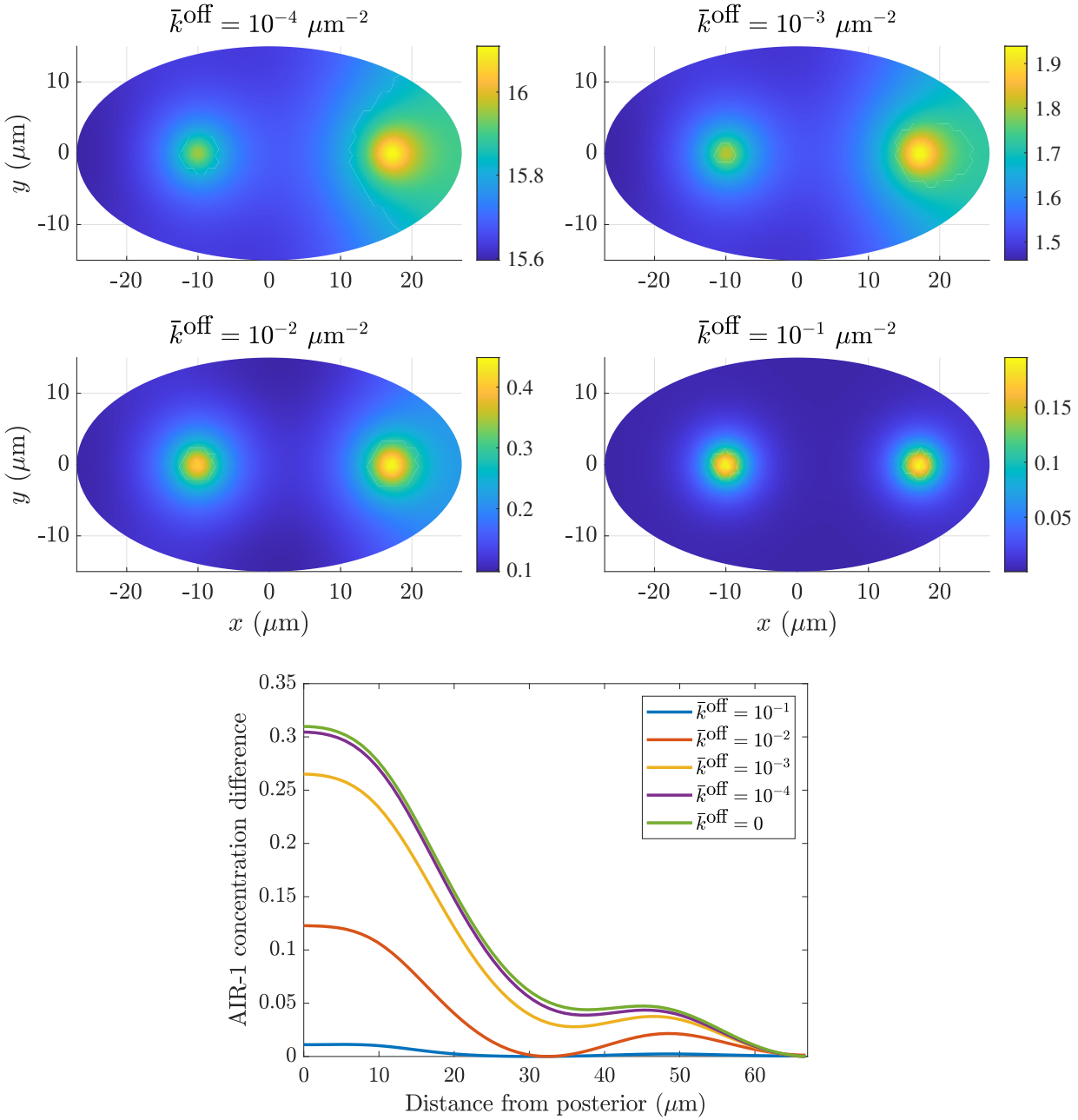

Figure 3: Profile of AIR-1 in wild-type embryo, obtained by solving (3) with different values of $\bar{k}^{\text{off}} = k^{\text{off}}/D$. The top plots show the profile along the whole embryo when changing $\bar{k}^{\text{off}}$; the bottom (summary) plot shows the change in the AIR-1 concentration (relative to the anterior pole) along the embryo perimeter.

inactivation rate leads to more of the AIR-1 being inactivated prior to reaching the posterior pole, which causes the gradient to drop (for $\bar{k}^{\text{off}} = 10^{-2}\ \mu\text{m}^{-2}$), and then vanish (for $\bar{k}^{\text{off}} = 10^{-1}\ \mu\text{m}^{-2}$).

2 The ECT-2 response

Let us now examine how the strength of the AIR-1 signal affects the strength of the ECT-2 concentration on the proximal cortex. To do so, let us suppose that ECT-2 locally binds and unbinds from the cortex, with AIR-1 increasing the unbinding rate. At steady state, this gives the equation

$$k_E^{\text{on}} = k_E^{\text{off}} \left(1 + K_{\text{AE}} \left(A - A_{\text{min}}\right)\right) E \to E = \frac{k_E^{\text{on}}/k_E^{\text{off}}}{1 + K_{\text{AE}} \left(A - A_{\text{min}}\right)} \tag{4}$$

where K_{AE} is the strength of AIR-1/ECT-2 inhibition, and A_{min} is the minimum level of AIR-1 across all embryo conditions. To fit the parameters in this model, we use the AIR-1 concentration data *with inactivation* (Section 1.1), so that the absolute concentrations are well defined. We set $\bar{k}^{\text{off}} = 10^{-3}\ \mu\text{m}^{-2}$, since this corresponds to a slight weakening of the diffusion without flattening the profile completely. This value of $\bar{k}^{\text{off}}$ results in the AIR-1 profiles shown in the left panel of Fig. 4. The parameter $A_{\text{min}} = 1.1$ is set to the minimum AIR-1 concentration across all embryos, and then $k_E^{\text{on}}/k_E^{\text{off}} = 2.5$ is obtained by fitting the maximum ECT-2 accumulation from experimental data (dhc-1 (RNAi) embryos). The last parameter $K_{\text{AE}} = 1.3$ is set to match the minimum ECT-2 accumulation of 0.8 when AIR-1 is at its maximum (about 2.8 in dhc-1 (RNAi) embryos). The right panel of Fig. 4 shows the resulting ECT-2 profiles we obtain across different conditions.

Figure 5 compares the resulting output (right panel) to the experimental data (left panel). While we can generally reproduce the trends observed experimentally, the shape of our curve appears to be more of a line, while the experimental data show an S-shaped trend. Indeed, while we correctly predict the ECT-2 accumulation for the "extreme" embryos (dhc-1 (RNAi) and zyg-9 (b224)/tpxl-1(RNAi)), the intermediate embryos have A/P ECT-2 disparities which are smaller than the experimental data. For example, in wild-type embryos, the experiments show an accumulation of 1.8 on the posterior, and 1 on the anterior, while our results show an accumulation of 1.7 on the posterior and 1.4 on the anterior.

Because we chose parameters to match dhc-1 (RNAi) embryos, their values are correct by design. If, by contrast, we had chosen a larger K_{AE} to match wild-type embryos, then the model results would be reversed: the wild-type embryos would be correct by design, while the extreme embryos would have A/P ratios which are much *larger* than the experiments. It seems clear that our model is missing a mechanism whereby either:

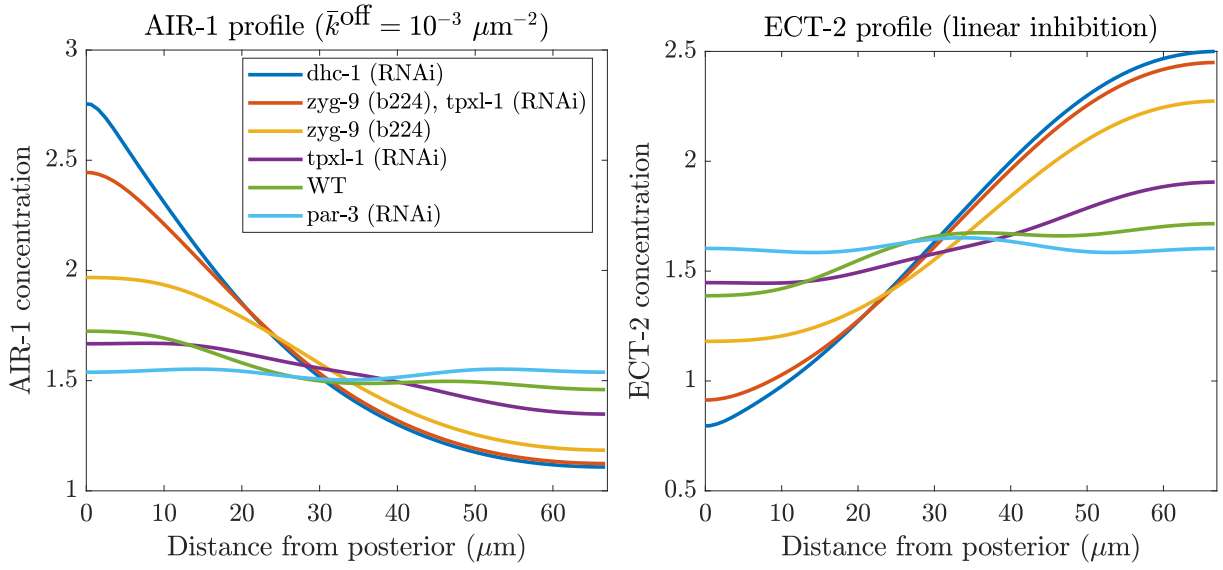

Figure 4: AIR-1 and ECT-2 profiles assuming linear inhibition model (4). The AIR-1 profiles are obtained by solving (3) with the different centrosome distances obtained from [5] and $\bar{k}^{\text{off}} = 10^{-3}$ μm^{-2}. The ECT-2 profiles are then obtained from (4), where we set $A_{\min} = 1.1$, $k_E^{\text{on}}/k_E^{\text{off}} = 2.5$, and $K_{\text{AE}} = 1.3$.

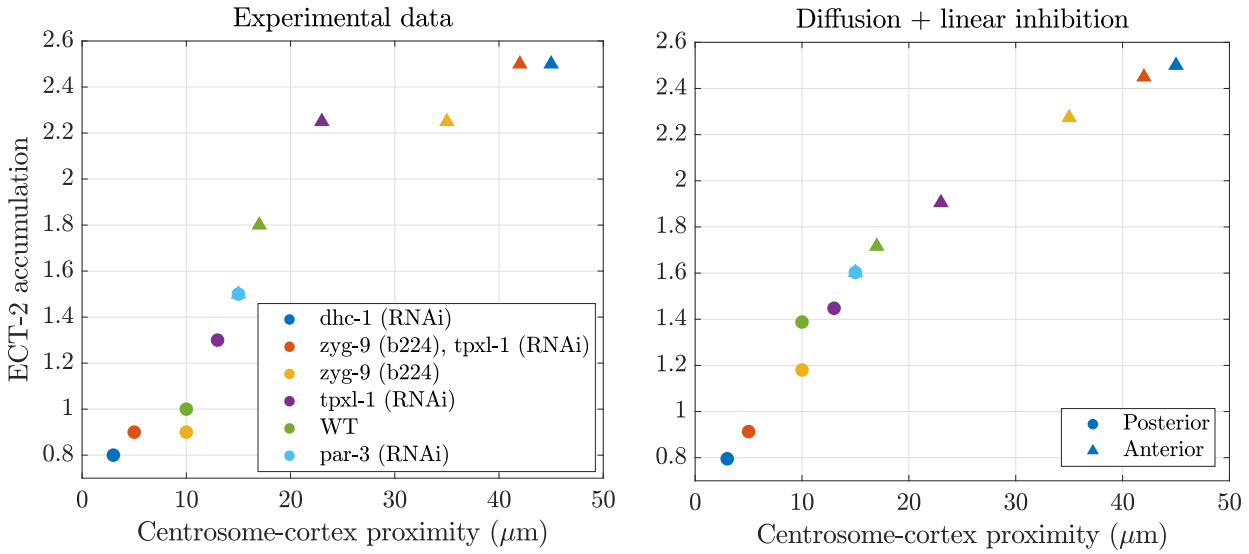

Figure 5: Comparing model results to experimental data for embryos with varying treatments (see legend at left). The left plot is a reproduction of [5, Fig. 7A], with some of the redundant embryo treatments deleted for clarity (we reduce multiple replicates to a single symbol by taking a rough average). The right plot shows the results when we consider diffusion of AIR-1 to the cortex, plus linear inhibition of the form (4) (see Fig. 4 for details).

1. Small changes in ECT-2 concentration induced by diffusion (in an intermediate range) are amplified to become larger.

2. Large changes in ECT-2 concentration induced by diffusion are damped to become smaller.

Since we have not accounted for the resulting actomyosin flows which tend to concentrate ECT-2, we speculate that the first of these options is what is missing from the model. We proceed to study it next.

2.1 Flows by myosin

We now explore the possibility that flows due to myosin could propagate smaller ECT-2 asymmetries into larger ones. To do this, we consider the basic model that ECT-2 (through activating ρ) activates myosin at the cortex. To minimze the number of parameters, we consider a simplified version of the true dynamics (where ECT-2 signals myosin by activating rho) and formulate a model with two variables, E (for ECT-2) and M (for myosin). In a system of units where length is in units of the embryo perimeter L, time is in units of the bound myosin lifetime $1/k_M^{\text{off}}$, and concentrations are scaled to be 1 when all protein is bound, the general equations governing this system can be written as

$$\partial_t E + \sigma_0 \partial_x \left(vE\right) = D_E \partial_x^2 E + K_E^{\text{on}} \left(1 + K_{\text{ME}} M\right) E_c - K_E^{\text{off}} \left(1 + K_{\text{AE}} \left(A - A_{\text{min}}\right)\right) E \tag{5a}$$

$$\partial_t M + \sigma_0 \partial_x \left(vM\right) = D_M \partial_x^2 M + K_M^{\text{on}} \left(1 + K_{\text{EM}} E\right) M_c - M - K_{\text{fb}} M(t-\tau)^4 \tag{5b}$$

$$v = \ell^2 \partial_x^2 v + \ell \partial_x M \tag{5c}$$

$$E_c = 1 - \int_0^1 E(x)\, dx \qquad M_c = 1 - \int_0^1 M(x)\, dx. \tag{5d}$$

The first two equations are advection-reaction-diffusion equations which describe the dynamics of ECT-2 and myosin. The term $\sigma_0 \partial_x \left(vE\right)$ describes the rate at which the ECT-2 concentration field is advected by the flow on the cortex, and likewise for the term $\sigma_0 \partial_x \left(vM\right)$ in the myosin equation. In the reaction terms, we assume that myosin recruits ECT-2 from the cytoplasm, and incorporate the term $K_{\text{ME}} M E_c$ in the ECT-2 equation. AIR-1 inhibits ECT-2 (by promoting unbinding) according to the relationship (4). For myosin, we assume a basal activation rate plus a rate proportional to the ECT-2 concentration (the term $K_{\text{EM}} E M_c$). We also assume delayed negative feedback of myosin via the term $K_{\text{fb}} M(t-\tau)^4$. This is an approximation of a more detailed mechanism whereby actin recruits RhoGAP, which inactivates Rho and myosin [7]. The velocity equation (5c) is a force balance equation where the active ($\partial_x M$) and viscous ($\partial_x^2 v$) forces are balanced by the drag force

(proportional to v) required to drag myosin at a velocity v through the cortex [1]. The variable ℓ is the hydrodynamic lengthscale (approximately 10 μm [6]).

2.1.1 Parameter estimation

A simple set of assumptions, some of which are based on experimental data, allows us to reduce the dynamics in (5) to two unknown parameters. We do this as follows,

1. The embryo cross section is an ellipse with approximate radii 27 μm and 15 μm, which gives a perimeter $L = 134.6$ μm [3] .

2. The myosin bound lifetime is about 8 s, so $k_M^{\text{off}} = 0.12/\text{s}$ [4].

3. We assume that all species have a dimensional diffusion coefficient $D = 0.1$ $\mu\text{m}^2/\text{s}$ [3, 4, 8]. Rescaling length by L and time by k_M^{off} gives a dimensionless coefficient $D_E = D_M = 0.1/(L^2 k_M^{\text{off}}) = 4.6 \times 10^{-5}$.

4. The ECT-2 lifetime was measured using FRAP to be on the order of a few seconds [5]. We set $k_E^{\text{off}} = 0.033$, for a three second lifetime. Rescaling gives $K_E^{\text{off}} = k_E^{\text{off}}/k_M^{\text{off}} = 0.033/0.12 = 0.275$.

5. The value of $K_{\text{ME}}M$ determines what fraction of ECT-2 binding occurs from recruitment by myosin. We assume that 50% of ECT-2 is recruited by myosin, so that $K_{\text{ME}}M = 1$. Because $M \approx 0.3$ (see assumption 7), we set $K_{\text{ME}} = 1/0.3$.

6. The value of $K_{\text{EM}}E$ determined what fraction of myosin activation occurs via the ECT-2 pathway. We assume that 2/3 of myosin is activated by ECT-2, so that $K_{\text{EM}}E = 2$. Because $E \approx 0.1$ (see assumption 7), we set $K_{\text{EM}} = 20$.

7. We assume that 10% of ECT-2 is bound to the cortex, and 30% of myosin is bound to the cortex [4, Fig. S3j]. This sets $K_E^{\text{on}} = 0.018$ and $K_M^{\text{on}} = 0.175$.

8. For the delayed negative feedback of myosin, we use the parameters determined in [7]. The model there considered rho (ρ) and RhoGAP (r) as the unknowns, with the production of RhoGAP proportional to ρ^3 and the inhibition of ρ proportional to $r\rho$. Here we coarse-grain this model into a single term, with the inhibition proportional to M^4. The time delay is approximately $\tau = 10$ s (rescaling by k_M^{off}, we get $\tau = 1.2$ in units of myosin lifetime), as obtained from experimental data [7]. The feedback strength is obtained by assuming an equilibrium of r in the equations of [7] (neglecting the basal binding rate), which gives (in

their notation) $K_{\text{fb}} = k_{\text{GAP}} \left(k_r^{\text{ass}}/k_r^{\text{diss}}\right) = 0.1(0.245/0.047) = 0.52/\text{s}$. Rescaling by k_M^{off} gives $K_{\text{fb}} = 4.3$ in our model.

This systematic fitting procedure reduces the dynamics to two parameters: K_{AE}, which describes the rate at which AIR-1 inhibits ECT-2, and σ_0, which is the speed of flows induced by myosin gradients. By manipulating these two parameters, we can model situations where ECT-2 gradients are due to AIR-1 alone (this is Fig. 5, where $K_{\text{AE}} = 1.3$ and $\sigma_0 = 0$), or where there is substantial amplification by flows. In the extreme case when $K_{\text{AE}} = 0$ and σ_0 is sufficiently large, we will get oscillatory dynamics, with peaks of myosin occuring at random places, in accordance with the model of [7]. We need a sufficiently large K_{AE} to ensure that the myosin peaks are in the right places.

Our approach is to start with a uniform concentration of ECT-2 and myosin, then apply the AIR-1 signal and watch the dynamics for ten minutes (long enough to reach a rough steady state, as shown in Fig. 6). To find a combination of K_{AE} and σ_0 that best satisfies the data, we start by fixing K_{AE}, then adjust σ_0 so that dhc-1 embryos have the experimental A/P ratio (≈ 3.2) of ECT-2 at the end of the simulation. We accept a pair of parameters $(K_{\text{AE}}, \sigma_0)$ if these same parameters give an A/P ratio around 1.8 in wild-type embryos as well. Figure 6 shows the dynamics over ten minutes with our chosen parameters $K_{\text{AE}} = 0.3$ and $\sigma_0 = 0.15$. In dhc-1 embryos, there is a single peak in the ECT-2 and myosin concentration which forms at around 75% embryo length (from the posterior), while in wild-type there are two peaks of ECT-2: one at the midline, and one at the anterior pole.

To compare our results with flow to the experimental data, we define an accumulation on the anterior cortex as the maximum ECT-2 concentration on the anterior 25% of the embryo length, and likewise for the posterior. Figure 7 shows how our asymmetry results compare to the experimental data. Compared to the previous data in Fig. 5, our data show more of an "S" shape, qualitatively (and quantitatively, for the most part) reproducing the shape obtained in experiments.

3 Polarization

Here we attempt to apply our model, with the same parameters, to the process of cell polarization. We begin with the diffusion calculation to establish the profile of AIR-1, then see how this propagates in our myosin/ECT-2 model.

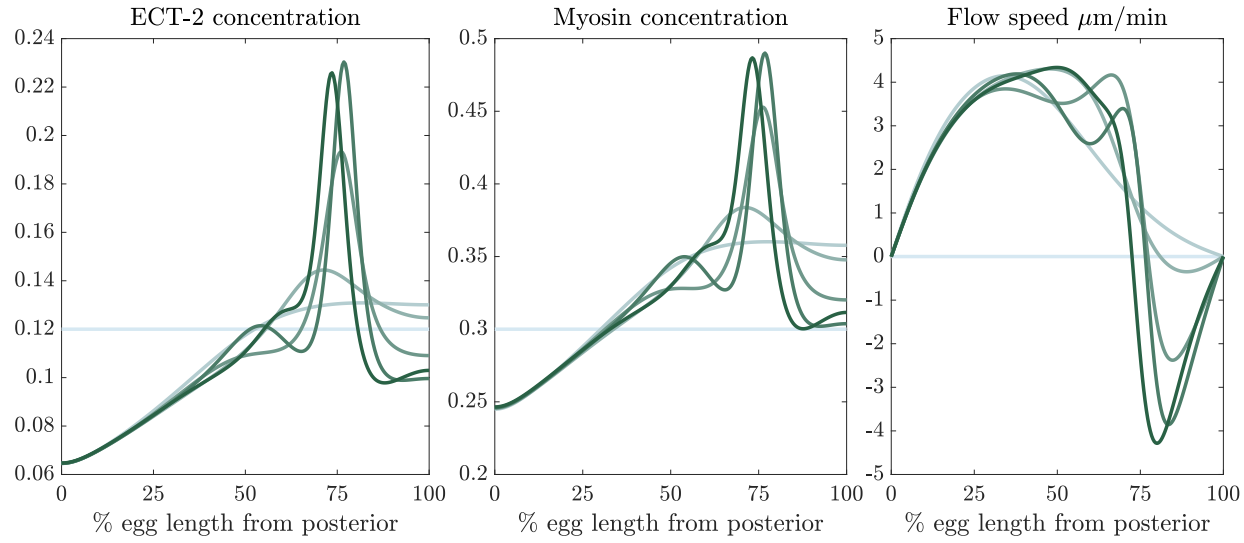

(a) dhc-1 (RNAi)

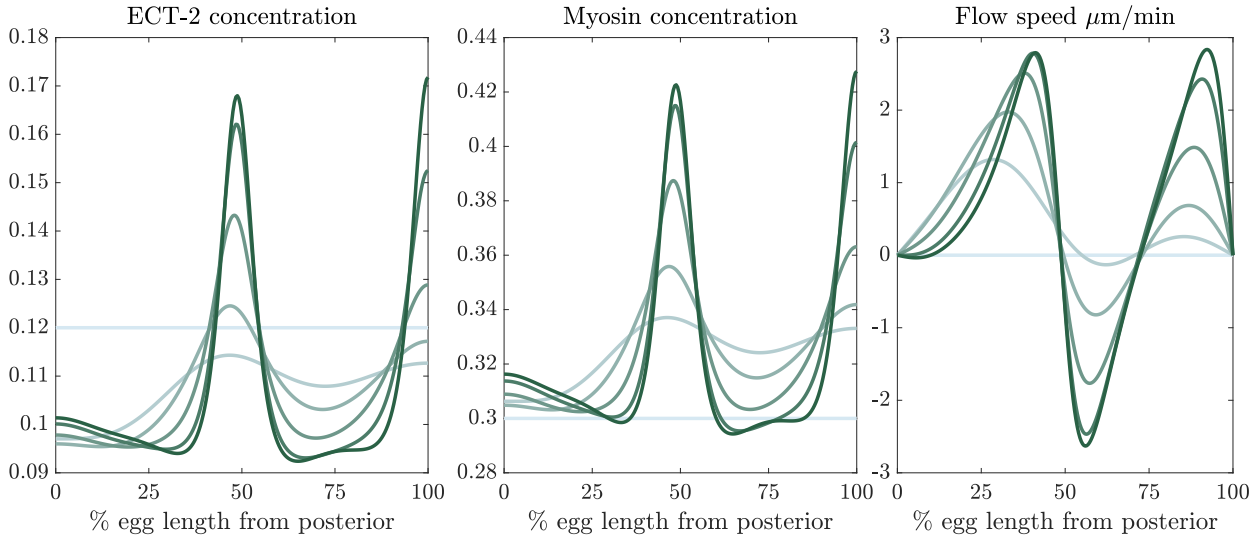

(b) Wild type

Figure 6: Trajectory with flows over 10 minutes of simulation time (cytokinesis conditions). We show the ECT-2 concentration, myosin concentration, and flow speed at times $t = 0$ (lightest lines), $t = 2, 4, 6, 8$, and $t = 10$ (darkest lines). (a) dhc-1 embryos, where the AIR-1 signal is stronger and concentrated almost entirely in the posterior (see Fig. 4). (b) Wild-type embryos, where the AIR-1 has a local minimum at the midline of the cell, plus an absolute minimum at the anterior pole.

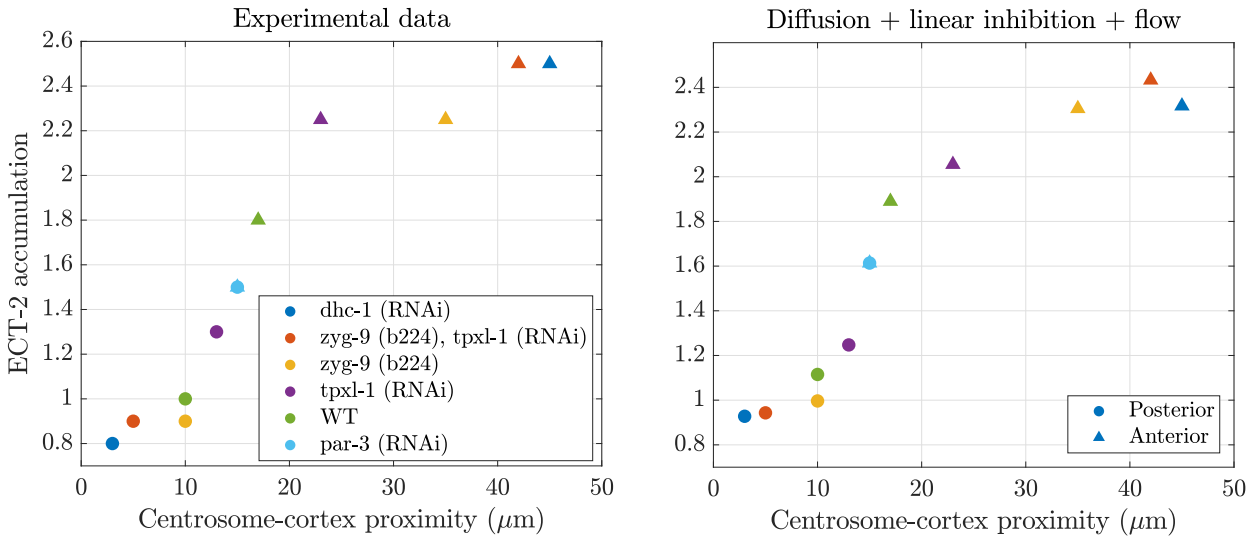

Figure 7: Comparing model results with myosin flows to experimental data for embryos with varying treatments (see legend at left). The left plot is a reproduction of [5, Fig. 7A], with some of the redundant embryo treatments deleted for clarity (we reduce multiple replicates to a single symbol by taking a rough average). The right plot shows the results when we consider diffusion of AIR-1 to the cortex, then run the model (5) to steady state with our chosen parameters. Unlike the model without flow (Fig. 5), the model with flow reproduces the "S" shape observed in experiments.

3.1 Diffusion of AIR-1

In cell polarization, *both* centrosomes sit very close to the posterior cortex (about 1 μm away [2]). The centrosomes have a smaller size (about 0.2 μm, so we set $\sigma_c = 0.1$ μm). They also contain substantially less total AIR-1; here we assume that the amount scales with the area, so that $C_0 = 0.01$ for polarization. Figure 8 shows the resulting AIR-1 concentration profile (the solution of (3) with $\bar{k}^{\text{off}} = 10^{-3}$ μm^{-2} once again) across the embryo and along the boundary. We observe a change in AIR-1 of only 0.03 from one side of the embryo to the other, which is substantially *smaller* than what we observed in cytokinesis. Considering that ECT-2 becomes asymmetrically enriched during polarization at the same levels as in cytokinesis, this underscores the need to have a mechanism to amplify the asymmetries.

3.2 The myosin response

We now simulate the response to the AIR-1 signal using the equations (5). We use all of the same parameters as for cytokinesis, with the exception of A_{min}, which is the "base" concentration of AIR-1, at which there is no effect on ECT-2. We previously set this value to be the smallest value of

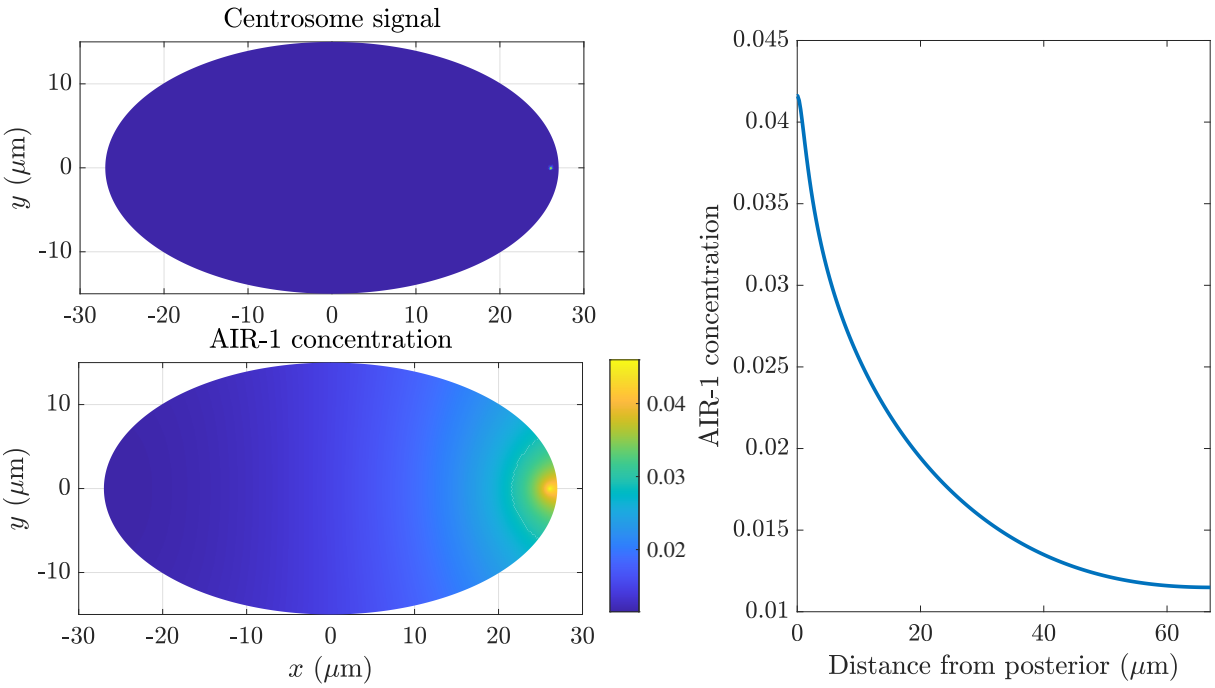

Figure 8: AIR-1 signal during polarization. In polarization, both centrosomes sit on the posterior cortex (we assume 1 μm away), have smaller size (about 0.2 μm, so we set $\sigma_c = 0.1$ μm), and contain less ($C_0 = 0.01$) AIR-1 than in cytokinesis (see plot at top left). The resulting concentration profile is shown across the entire embryo (bottom left) and along the embryo boundary (right).

the AIR-1 concentration across all embryos in cytokinesis; here we use the minimum concentration for polarization, which, according to Fig. 8 is $A_{\min} = 0.01$.

Figure 9 shows the response of the system to the AIR-1 signal, which in polarization is highly localized to the posterior cortex (see Fig. 8). In the first ten minutes of simulation time (which is longer than polarity establishment phase), a peak in myosin and ECT-2 forms immediately next to the posterior pole. At $t = 10$ minutes, this peak has an A/P asymmetry of roughly 2. Later times show formation of additional peaks, and a steady state emerges with a set of three peaks of the same size. The overall ECT-2 asymmetry is roughly 2.5, which is slightly larger than what is measured experimentally (at most 1.8).

The major qualitative issue with this model is the location of the peaks, and the inability to move the peak that initially forms near the posterior pole. In experiments, we might expect the dynamic reorganization of PAR proteins to shift the location of the peak in ECT-2. Because this model does not account for PAR proteins, peaks that initially form at a fixed location will not move, because the signals upstream of them do not change. The result is the profiles shown in Fig. 9.

References

[1] Justin S Bois, Frank Jülicher, and Stephan W Grill. Pattern formation in active fluids. *Biophysical Journal*, 100(3):445a, 2011.

[2] Carrie R Cowan and Anthony A Hyman. Centrosomes direct cell polarity independently of microtubule assembly in c. elegans embryos. *Nature*, 431(7004):92–96, 2004.

[3] Nathan W Goehring, Philipp Khuc Trong, Justin S Bois, Debanjan Chowdhury, Ernesto M Nicola, Anthony A Hyman, and Stephan W Grill. Polarization of par proteins by advective triggering of a pattern-forming system. *Science*, 334(6059):1137–1141, 2011.

[4] Peter Gross, K Vijay Kumar, Nathan W Goehring, Justin S Bois, Carsten Hoege, Frank Jülicher, and Stephan W Grill. Guiding self-organized pattern formation in cell polarity establishment. *Nature physics*, 15(3):293–300, 2019.

[5] Katrina M Longhini and Michael Glotzer. Aurora a and cortical flows promote polarization and cytokinesis by inducing asymmetric ect-2 accumulation. *Elife*, 11:e83992, 2022.

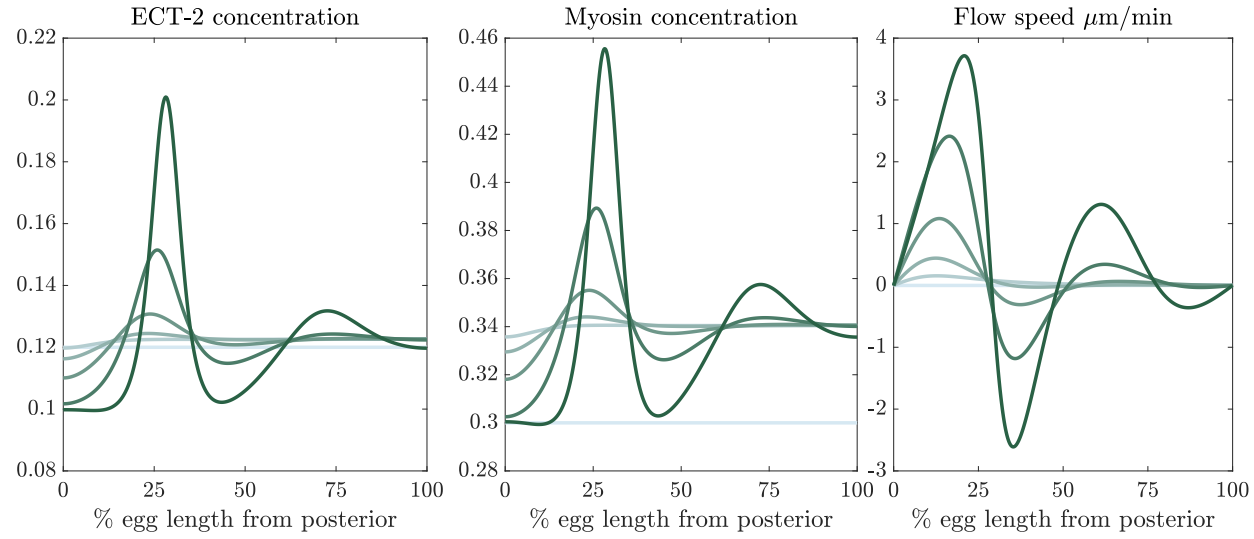

(a) First 10 minutes (establishment phase)

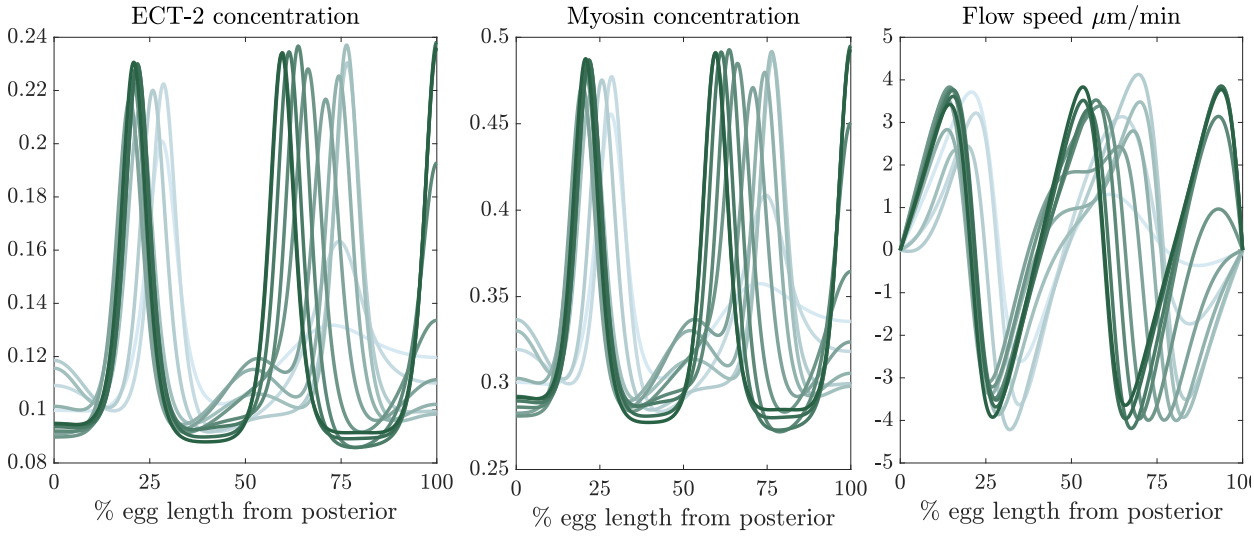

(b) Next 20 minutes (to steady state)

Figure 9: Dynamics for cell polarization model. We run the model (5), which we previously fit to cytokinesis, with the same parameters, changing only the AIR-1 profile to the polarization cue obtained in Section 3.1. We show the dynamics at two minute intervals, starting from $t = 0$, over (a) the first ten minutes (which is at most the length of polarity establishment phase) and (b) the next twenty minutes (which establishes a steady state but is of little relevance in practice). Darker lines show later times.

[6] Mirjam Mayer, Martin Depken, Justin S Bois, Frank Jülicher, and Stephan W Grill. Anisotropies in cortical tension reveal the physical basis of polarizing cortical flows. *Nature*, 467(7315):617–621, 2010.

[7] Jonathan B Michaux, François B Robin, William M McFadden, and Edwin M Munro. Excitable rhoa dynamics drive pulsed contractions in the early c. elegans embryo. *Journal of Cell Biology*, 217(12):4230–4252, 2018.

[8] François B Robin, William M McFadden, Baixue Yao, and Edwin M Munro. Single-molecule analysis of cell surface dynamics in caenorhabditis elegans embryos. *Nature methods*, 11(6):677–682, 2014.